

03,05,11

Turning of activation energy and magnetoimpedance by alternating current frequency in manganese sulfide with partial substitution by samarium ions

© S.S. Aplesnin, A.M. Kharkov, M.N. Sitnikov

Siberian State University of Science and Technology,
Krasnoyarsk, Russia

E-mail: apl@iph.krasn.ru

Received August 21, 2023

Revised August 21, 2023

Accepted October 5, 2023

The dynamic characteristics of the $\text{Sm}_x\text{Mn}_{1-x}\text{S}$ solid solution are studied by impedance spectroscopy in the frequency range of 10^2 – 10^6 Hz, IR spectroscopy in the temperature range of 80–500 K. The relaxation time of current carriers and its dependence on temperature from the impedance hodograph are found. A correlation between the temperatures of anomalies in the transport characteristics and the frequency of softening of the IR vibration mode of the octahedron is established. The frequency dependence of the activation energy and the critical frequency of the transition from semiconductor to metallic type of conduction are found. The reversal of the sign of the magnetoimpedance and magnetoresistance on alternating current in $\text{Sm}_x\text{Mn}_{1-x}\text{S}$ upon heating and their maximum in the region of the electronic structural transition are determined. The magnetoimpedance in the paraphase is explained by the change in the permittivity in a magnetic field.

Keywords: semiconductors, impedance, magnetoimpedance.

DOI: 10.61011/PSS.2023.11.57312.186

1. Introduction

Controlling transport characteristics in semiconductors exposed to an external magnetic field is of interest from both fundamental and practical points of view. In electrically inhomogeneous semiconductors, the transport characteristics under direct and alternating current in a magnetic field can be qualitatively different. In the region of p – n junction in Si at room temperature in a magnetic field of 5 T, a large magnetoresistive effect is observed [1,2], which is due to the redistribution of space charge in the region of junction. With alternating current, an electrical capacitance is added, which also changes in the magnetic field. The magnetic capacitance effect in $\text{Ho}_x\text{Mn}_{1-x}\text{S}$ semiconductors depends on the radius of the inhomogeneity and the relaxation time of current carriers, which is determined by the interaction with the magnetic and elastic subsystems [3]. The electrical heterogeneity can be controlled by changing valence, concentration, and temperature.

The change in valence is achieved through chemical pressure when the concentration changes. For example, in a system with anionic substitution of $\text{TmSe}_{1-x}\text{Te}_x$ the transition from divalent TmTe to trivalent TmSe is achieved at $x = 0.4$ (a gap opens with an energy of 0.04 eV [4,5]). The exchange-induced valence transition was studied in $\text{Tm}_{1-x}\text{Eu}_x\text{Se}$ [6]. Eu chalcogenides exhibit exchange splitting of the $5d$ -conduction band in a magnetic-ordered state, which results in a shift of the bottom of the conduction band („red shift“) and in a decrease in the gap between localized $4f$ -states and band $5d$ -states. At 300 K, when

the concentration of europium ions $x = 0.2$ exceeds the percolation concentration $x_c = 0.17$, a gap opens between the $5d$ -band and the $4f^{13}$ -state, with width of this gap varying from 40 to 160 meV. The lattice constant up to the concentration of $x = 0.2$ corresponds to Tm^{3+} , above the concentration of $x = 0.4$ it corresponds to Tm^{2+} and at low temperatures of $T < 50$ K the thulium valence increases to $\text{Tm}^{2.175+}$ [7].

In manganese sulfide, when manganese is substituted with samarium ions of mixed valence, fluctuations in the charge state are possible. Manganese sulfide is a magnetic semiconductor with a Néel temperature of 150 K, a gap in the spectrum of electronic excitations of 3 eV [8]. Samarium sulfide belongs to semiconductors with intermediate valence and at a pressure of 5.6 kbar it transforms into the metallic state as a result of lattice compression and a decrease in the lattice constant a from 0.597 down to 0.569 nm [9,10]. The valency of samarium depends on the magnitude of hybridization of the $4f$ -band and the $5d$ -band and on the width of the $4f$ -level. Depending on the content of Sm ions in the cluster (for example, the cluster may consist of single Sm ions), dimers in the manganese sulfide matrix with the lattice parameter of $a = 0.521$ nm have different chemical pressure from manganese ions. Fluctuations in the samarium valence in $\text{Mn}_{1-x}\text{Sm}_x\text{S}$ are possible being accompanied by local lattice deformations. When heated, the chemical pressure on samarium ions changes from the side of the MnS matrix, whose thermal expansion coefficient is $2 \cdot 10^{-5} \text{ K}^{-1}$ [11]. For example, small structural distortions leading to a volume change of

0.48% in the LK-99 material result in the room-temperature superconductivity [12]. In SmS, the hybridization of f and d states results in the formation of excitons [13]. In the solid solution of $\text{Mn}_{1-x}\text{Sm}_x\text{S}$, the formation of excitons leads to the degeneracy of the t_{2g} shell, which is removed by the crystal field of the octahedron during its deformation and by the magnetic field. That is, the topology of an electrically inhomogeneous state changes in a magnetic field, which leads to a change in the frequency dependence of the dielectric constant in the magnetic field, and the prerequisites for magnetoelectricity are created.

2. Materials and IR spectroscopy

The phase composition and crystal structure of the $\text{Mn}_{1-x}\text{Sm}_x\text{S}$ sample were studied in a DRON-3 X-ray set-up using $\text{CuK}\alpha$ -radiation at room temperature. Figure 1 shows an X-ray diffraction pattern of the sample. Peaks arising because of the reflection from planes parallel to Z axis, with Miller indices of $(hk0)$, can be approximated by two lines, the distance between which exceeds the fitting error. For example, peak (220) is split into two peaks with $2\Delta\theta = 48.85(2)$ and $48.89(2)$. The error in approximating peaks (hkl) by two lines exceeds the distance between them. The intensities of the split X-ray lines (inset in Figure 1) differ by an order of magnitude, and they can be attributed to the lattice constants of $a(\text{Mn-Sm})/a(\text{Mn-Mn}) = 0.0008$, which differ by 0.08%. According to the results of X-ray diffraction analysis, the synthesized compounds have a cubic lattice of the NaCl type with a lattice constant of $a = 0.526$ nm. This suggests that samarium cations remain close to the trivalent state, because linear interpolation to $x = 1$ yields $a = 0.566$ nm.

Impedance, active and reactive parts of the impedance were measured by an AM-3028 component analyzer in a frequency range of $\omega = 10^2 - 10^6$ Hz at temperatures of 80–400 K, the AC voltage amplitude was 1 V. Impedance spectra were calculated using the ZView software (Scribner Associates Inc.). Electrical resistance was measured by the four-contact method in a temperature range of 80–500 K on a Keysight 3458A multimeter, the IR spectrum was obtained using a FSM2202 Fourier spectrometer with a resolution of 0.5 cm^{-1} .

The correlation of structural and electronic transitions will be determined from the IR spectra. For example, an electronic transition in vanadium oxides entails changes in the structure, which appear in Raman spectra and IR spectra [14]. Or a decrease in the symmetry of the crystal leads to a restructuring of the electronic spectrum. The solid solution of $\text{Sm}_{0.1}\text{Mn}_{0.9}\text{S}$ is electrically inhomogeneous, contains SmS clusters, ionic radii and bond lengths of Sm–S–Sm, Mn–S–Mn, and Sm–S–Mn are different. Therefore, from the IR spectra it is possible to determine local distortions of the structure in the region where samarium ions are located. Figure 2 shows the IR spectra of $\text{Sm}_{0.1}\text{Mn}_{0.9}\text{S}$.

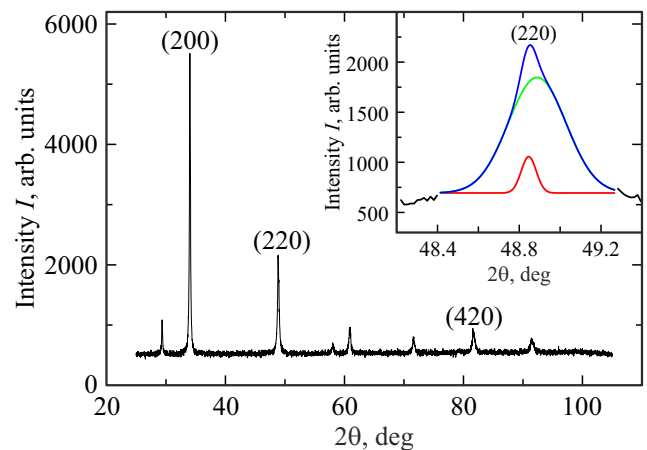


Figure 1. X-ray diffraction pattern of $\text{Sm}_{0.1}\text{Mn}_{0.9}\text{S}$ sample. The inset shows a fit of peak (220) with two Gaussian lines.

In the frequency range of $550 - 650 \text{ cm}^{-1}$, a vibration mode was found that is absent in manganese sulfide and is caused by octahedra containing ionic bonds of Sm–S–Mn and Sm–S–Sm. In LiCl–KCl chloride systems the vibration frequency of the octahedron is $\text{Sm}^{2+} \omega = 425 \text{ cm}^{-1}$, and for the trivalent $\text{Sm}^{3+} \omega = 572 \text{ cm}^{-1}$ [15]. In pyrochlores, in the frequency region of $570 - 650 \text{ cm}^{-1}$, a stretching vibration mode of the SnO_6 octahedron [16,17] is observed in the Raman spectra and IR spectra. In $\text{La}_{0.67}\text{Pr}_{0.03}\text{Ca}_{0.2}\text{Sr}_{0.1}\text{MnO}_3$ and $\text{La}_{0.67}\text{Er}_{0.03}\text{Ca}_{0.2}\text{Sr}_{0.1}\text{MnO}_3$ manganites, in the Raman spectra the E_g -mode with $\omega = 610 \text{ cm}^{-1}$ was found, which is characterized by vibrations of the Mn–O and O–Mn–O bonds [18,19]. In the $\text{Bi}_2\text{Fe}_4\text{O}_9$ mullite, the Ag-mode of the octahedron with $\omega = 595 \text{ cm}^{-1}$ was calculated with the displacement of four oxygen ions in XY plane [20]. Structural defects in pyrochlores reduce local symmetry and allow electronic transitions that are absent in the parent compound [21,22].

The temperature dependence of the frequency of IR absorption maximum exhibits a number of anomalies (Figure 2). When heated above 100 K, the vibration frequency sharply decreases in the antiferromagnetic phase to the Néel temperature of $T_N = 140$ K, which is associated with a decrease in the contribution of the magnetic elastic interaction to the effective elastic modulus. In the interval of 220–240 K, the shift in the frequency of octahedral vibration mode by 2.5 cm^{-1} is caused by a local structural transition. Structural transitions of the shear type are observed in the crystal of Rb_2KInF_6 perovskite, where a change in symmetry occurs due to the rotation of the InF_6 octahedra [23]. The phase transition from the cubic phase G_0 to the tetragonal phase G_1 is a second-order transition, the phase transition from the phase G_1 to the monoclinic phase G_2 is a first-order transition, they are accompanied, respectively, by rotation through an angle of ϕ and have the form of $(0, 0, \phi)$ for the $G_0 - G_1$ transition and (ψ, ϕ, ϕ) for the $G_1 - G_2$ transition. It can be assumed that the change in

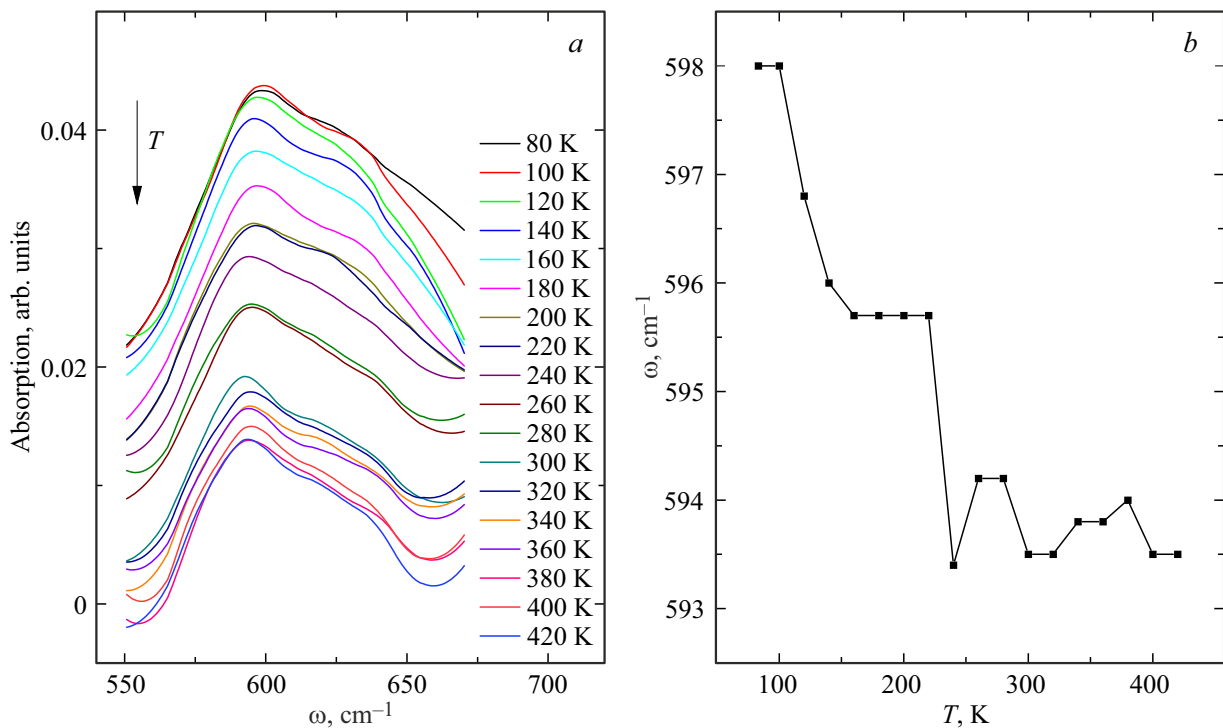


Figure 2. IR spectrum of $\text{Sm}_{0.1}\text{Mn}_{0.9}\text{S}$ at different temperatures (a) and frequency of the maximum IR absorption as a function of temperature (b).

the elastic modulus occurs due to the rotation of octahedra with Sm–S–Mn and Sm–S–Sm bonds. At temperatures of 300 and 375–400 K there is a tendency for the frequency to change, which is within the measurement error. It is possible that these changes are also caused by local deformations of regions with samarium ions.

3. Conductivity and impedance

In the solid solution of $\text{Sm}_{0.1}\text{Mn}_{0.9}\text{S}$, conductivity is due to the electrons of samarium ions, therefore local deformations will be manifested in conductivity and in impedance. Figure 3 shows the conductivity of polycrystalline samples of $\text{Sm}_{0.1}\text{Mn}_{0.9}\text{S}$ as a function of temperature.

The conductivity jump temperatures $T = 96, 232$ and 365 K correlate with anomalies in the IR spectra. At 96 K, spin polarons self-localize with the formation of ferrons, which leads to a tunnel type of conductivity with an activation energy of $dE = 8.3$ meV and to a decrease in resistance (inset in Figure 3). The jump of $\sigma(T)$ at 166 K is caused by a decrease in the symmetry of manganese sulfide to rhombohedral, which is consistent with the temperature of the thermal expansion coefficient maximum of MnS at 165 K [24]. An increase in conductivity by 55% at 232 K is caused by a local structural distortion in the vicinity of samarium ions, which causes a redistribution of the spectral density of electronic impurity states at the level of chemical potential.

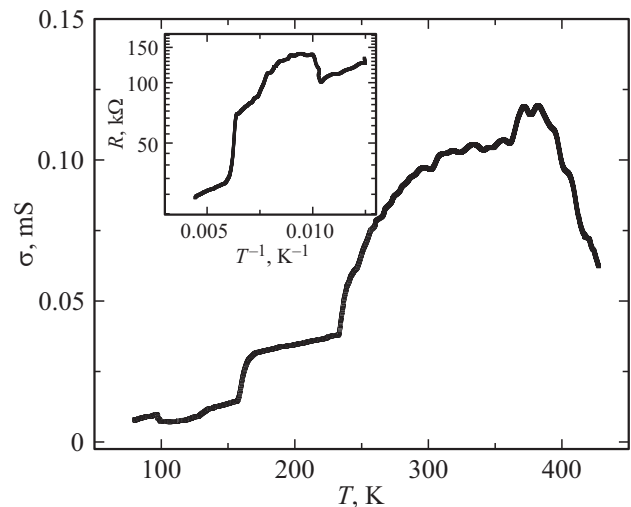


Figure 3. Conductivity of $\text{Sm}_{0.1}\text{Mn}_{0.9}\text{S}$ as a function of temperature. Inset: resistance as a function of reciprocal temperature.

The mechanism of current carrier scattering can be determined from the impedance. Figure 4 shows the impedance components of $\text{Sm}_{0.1}\text{Mn}_{0.9}\text{S}$ as a function of temperature. Based on the impedance the dynamic characteristics of current carriers and relaxation time will be found.

It can be seen from the $\text{Re}(Z(T))$ dependences that at frequencies below a certain critical frequency ω_c the resistance decreases when heated. At $\omega > 10^4$ Hz, the resistance increases when heated to a temperature of 232 K.

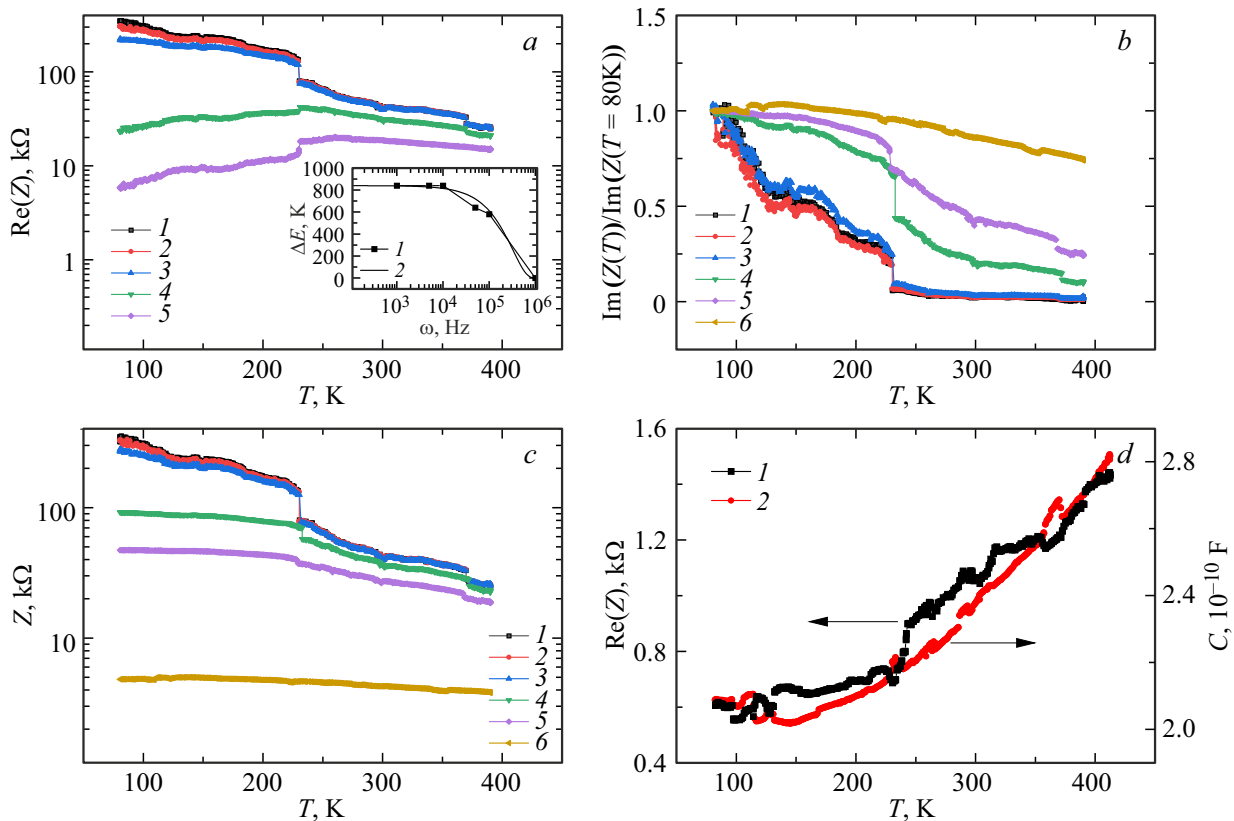


Figure 4. Real (a) and normalized imaginary (b) parts of the impedance Z (c) depending on temperature at frequencies of $\omega = 1$ (1), 5 (2), 10 (3), 50 (4), 100 (5), 1000 (6) kHz for $\text{Sm}_{0.1}\text{Mn}_{0.9}\text{S}$. Active resistance (1) and capacitance (2) at a frequency of $\omega = 1$ MHz (d). Inset — activation energy ΔE as a function of frequency ω : 1 — experiment, 2 — approximating dependence $\Delta E = \Delta E_0(\omega_c - \omega)^3$.

With an increase in frequency above 100 kHz, the active part of the impedance increases with heating throughout the entire temperature range studied (Figure 4, d). Reactance is caused by the capacitance, i.e. $X = \text{Im}(Z) = 1/\omega C$, $C = 1/\omega X$. Below the Néel temperature, where the temperature coefficient of resistance is maximum, $\text{Re}(Z(T))$ increases sharply at frequencies of $\omega < \omega_c$ and decreases at $\omega > 10^4$ Hz. At the boundary of the Sm–S–Mn region, localized hole states arise as a result of screening of $\text{Sm}^{2+\delta}$ samarium ions. The resistance in the high frequency region exhibits dispersion and the conduction is caused by dielectric losses $\sigma(\omega) = \omega\epsilon_0 \text{Im}(\epsilon(\omega))$ in a local region with activation barriers at the boundaries of Sm–S–Mn [25]. A similar transition from activation conductivity to the metallic type of conductivity was observed in single crystals of the $\text{PbNi}_{1/3}\text{Nb}_{2/3}\text{O}_3$ relaxor ferroelectric above the ferroelectric transition temperature at a frequency of 100 kHz [26]. The activation barrier is due to the accumulation of charge at the boundaries as a result of hole diffusion under the effect of an external field, and with increasing frequency of the external alternating electric field, the activation energy is approximated by the exponential function of $\Delta E = \Delta E_0(\omega_c - \omega)^3$ (inset in Figure 4, a).

The relaxation time of current carriers will be found from the frequency dependence of the impedance. Figure 5

shows the real and imaginary parts of the impedance as a function of frequency.

The impedance components are well described by the Debye model:

$$\text{Re}Z(\omega) = \frac{A}{1 + (\omega\tau)^2}, \quad \text{Im}Z(\omega) = \frac{B\omega\tau}{1 + (\omega\tau)^2}, \quad (1)$$

where τ is current carrier relaxation time, A and B are parameters.

The relaxation time decreases in the temperature region of 80–100 K and has a minimum at 100 K, where the conductivity demonstrates a jump. The greatest changes in relaxation time are observed in the region of the magnetic phase transition as a result of the interaction of charge carriers with the magnetic subsystem and in the vicinity of the structural transition due to interaction with the elastic subsystem. The relaxation time at temperatures above 240 K changes slightly with heating, and has a small minimum at 375 K.

The impedance hodograph (Figure 6) is described in the equivalent-circuit model with a parallel connection of a capacitor and a resistor, that is, the relaxation of charge carriers is associated with the effective formation of a capacitive charge within the time of $\tau = RC$.

The effect of the magnetic field on the dynamic characteristics of current carriers was assessed by changes in

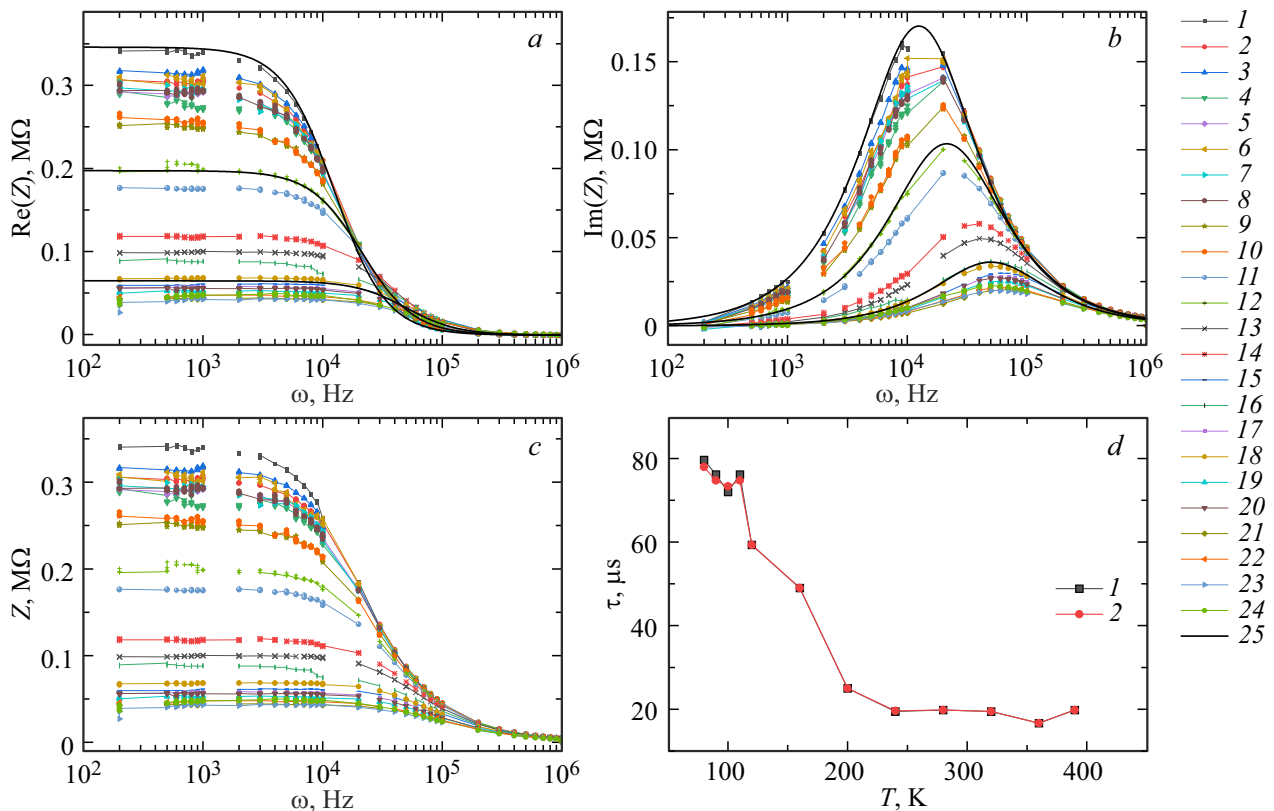


Figure 5. Frequency dependence of the real (a) and imaginary (b) parts of the impedance Z (c) for the $\text{Sm}_{0.1}\text{Mn}_{0.9}\text{S}$ sample in a zero magnetic field (1, 3, 5, 7, 9, 11, 13, 15, 17, 19, 21, 23) and in a magnetic field of $H = 12$ kOe (2, 4, 6, 8, 10, 12, 14, 16, 18, 20, 22, 24) at temperatures of $T = 80$ (1, 2), 90 (3, 4), 100 (5, 6), 110 (7, 8), 120 (9, 10), 160 (11, 12), 200 (13, 14), 240 (15, 16), 280 (17, 18), 320 (19, 20), 360 (21, 22), 390 (23, 24) K, as well as fitting functions (25) in the Debye model (1). (d) — Temperature dependence of relaxation time τ .

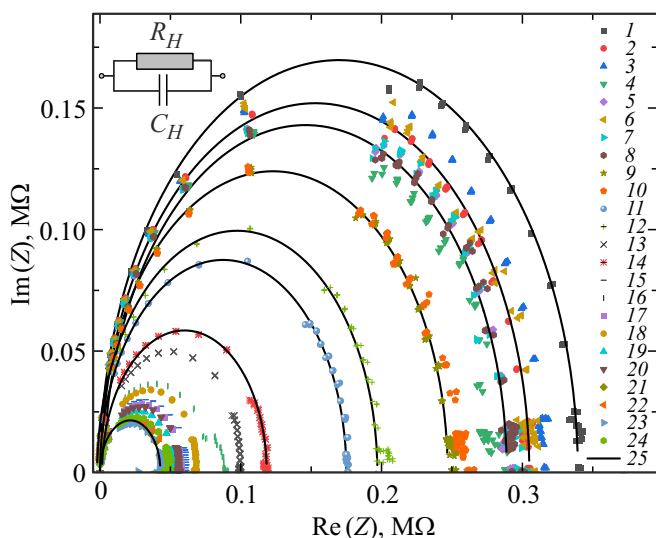


Figure 6. Impedance hodographs for the $\text{Sm}_{0.1}\text{Mn}_{0.9}\text{S}$ sample in a zero magnetic field (1, 3, 5, 7, 9, 11, 13, 15, 17, 19, 21, 23) and in a magnetic field of $H = 12$ kOe (2, 4, 6, 8, 10, 12, 14, 16, 18, 20, 22, 24) at temperatures of $T = 80$ (1, 2), 90 (3, 4), 100 (5, 6), 110 (7, 8), 120 (9, 10), 160 (11, 12), 200 (13, 14), 240 (15, 16), 280 (17, 18), 320 (19, 20), 360 (21, 22), 390 (23, 24) K. Fitting functions in the equivalent-circuit model (25). Inset: equivalent circuit using R_H , C_H — resistor and capacitor.

the impedance components in the magnetic field at fixed temperatures

$$\Delta R = (\text{Re}(Z(H, \omega)) - \text{Re}(Z(H=0, \omega))) / \text{Re}(Z(H=0, \omega));$$

$$\Delta Z = (Z(H, \omega) - Z(H=0, \omega)) / Z(H=0, \omega). \quad (2)$$

Figure 7 shows the dependences of alternating current magnetoresistance and magnetoimpedance on frequency. At frequencies lower than the relaxation frequency, the impedance and its components decrease in a magnetic field by 10% at $T < 100$ K and increase at $\omega > \omega_c$. With an increase in temperature at $T > 110$ K, the impedance and $\text{Re}(Z)$ increase in a magnetic field, the maximum increase of 50% is achieved at 240 K. Further heating leads to a decrease in the magnetic impedance (Figure 7, c).

4. Model

The impedance of $\text{Sm}_{0.1}\text{Mn}_{0.9}\text{S}$ in the paramagnetic phase increases in a magnetic field and reaches its maximum in the temperature range of the local electronic structural transition (Figure 7, c). The increase in impedance is caused by a decrease in the diagonal component of the dielectric constant in the magnetic field. The conductivity

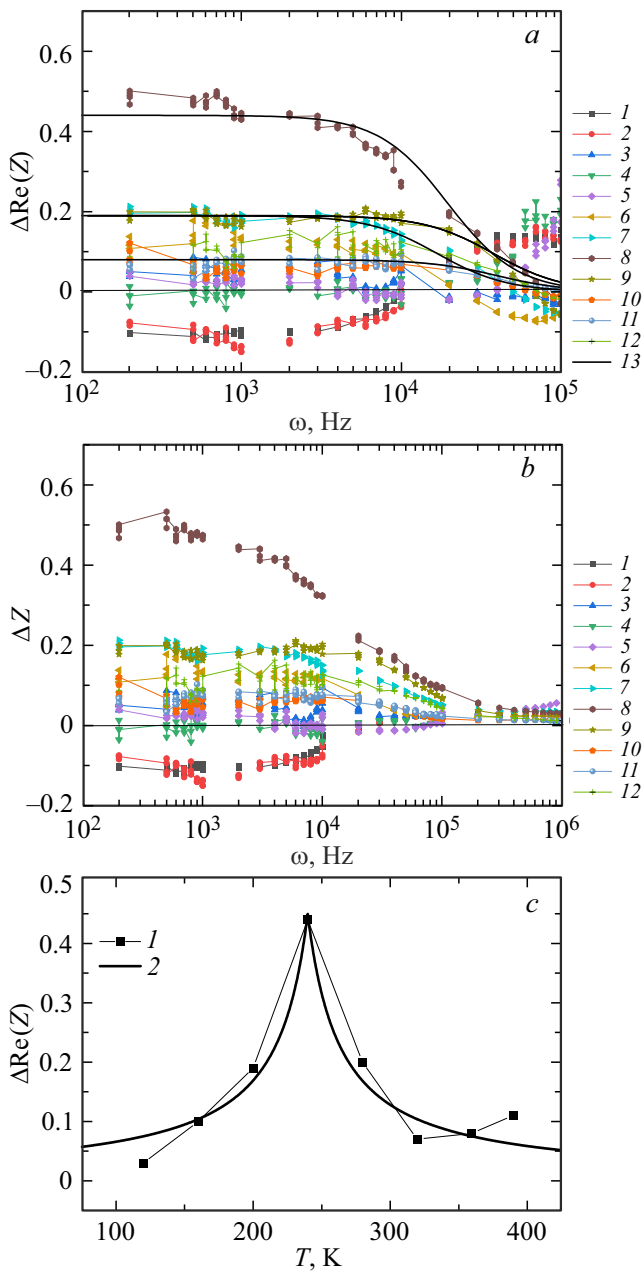


Figure 7. AC magnetoresistance (a) and magnetoimpedance ΔZ (b) as a function of frequency for the $\text{Sm}_{0.1}\text{Mn}_{0.9}\text{S}$ sample in a magnetic field of $H = 12$ kOe at temperatures of $T = 80$ (1), 90 (2), 100 (3), 110 (4), 120 (5), 160 (6), 200 (7), 240 (8), 280 (9), 320 (10), 360 (11), 390 (12) K. The solid line in part a is a fitting function according to formula (4). (c) Magnetoresistance at a frequency of $\omega = 1$ kHz as a function of temperature (1) and fitting function according to formula (5) (2).

is proportional to the dielectric constant $\sigma(\omega) = i\omega\epsilon$, impedance is $Z^2 = 1/\sigma^2 + 1/(\omega C)^2 \approx 1/\epsilon^2$. In an electrically inhomogeneous medium, the longitudinal component of the dielectric constant has the following form [27]:

$$\text{Re}[\epsilon_{xx}(\omega)] = \frac{\epsilon(1 - \beta^2 + (\omega\tau)^2(1 + \beta^2)^2)}{1 + (\omega\tau)^2(1 + \beta^2)^2}, \quad (3)$$

where $\beta = \mu H$, μ being mobility, $\tau = RC$. Relative change in the impedance

$$\frac{(Z(H) - Z(0))}{Z(H)} = \frac{(\epsilon(0) - \epsilon(H))}{\epsilon(0)} = \frac{\beta^2}{1 + (\omega\tau)^2(1 + \beta)^2} \quad (4)$$

and in its component is satisfactorily described by this function at frequencies of $\omega < \omega_c$ (Figure 7). The maximum of magnetoresistance and magnetoimpedance at 240 K is caused by an electronic-structural transition, in the region of which the mobility of charge carriers in a magnetic field changes similar to the correlation radius:

$$\mu \sim \xi = A/(|1 - T/T_0 + \Delta T|). \quad (5)$$

This function satisfactorily describes the experiment with the following parameters: $A = 0.045$, $T_0 = 240$ K, $\Delta T = 0.08$.

In the antiferromagnetic state, ferrons with local magnetization are formed in the vicinity of Sm ions. The accumulation of charge in the vicinity of a ferron leads to spin polarization of current carriers, and electron transitions between ferrons depend on the direction of localized momenta, which can be varied by a magnetic field. To estimate the magnetoresistance, the model of spin-polarized electron tunneling between quantum well can be used [28]:

$$\Delta R = \frac{(R(H) - R(0))}{R(0)} = \frac{1}{(1 + xP_1P_2 \cos \theta)} - 1, \quad (6)$$

where x is concentration of wells (ferrons), $P_{1,2}$ is degree of electronic polarization, θ is angle between localized momenta. For $x = 0.1$ and a polarization degree of $P_{1,2} = 1$ we get $\Delta R = -0.1$, and the model qualitatively describes the experiment. At a frequency of $\omega > \omega_c$, exceeding the relaxation frequency, the depolarizing charge of holes disappears and the resistance increases due to the Hall effect.

5. Conclusion

In manganese sulfide substituted with a samarium ion of mixed valence, a correlation was found between the softening temperatures of the octahedral vibration mode and conductivity jumps. The relaxation time of charge carriers was found from the impedance spectrum; its sharp decrease is observed during the transition from the antiferromagnetic state to the paramagnetic state. The critical frequency of transition from semiconductor type of conductivity to metallic type and from bulk to local conductivity in $\text{Sm}_x\text{Mn}_{1-x}\text{S}$ has been established. From the transport characteristics and IR spectra, an electronic structural transition below room temperature was found. A decrease in alternating current resistance and impedance in a magnetic field in the antiferromagnetic state was discovered at frequencies lower than the relaxation frequency, which is explained in the model of spin-polarized electron tunneling. Alternating current magnetoimpedance and magnetoresistance reach

maxima in the vicinity of the electronic-structural transition, which is due to the maximum mobility of current carriers in the magnetic field.

Funding

The study was supported by the Russian Science Foundation, the Government of the Krasnoyarsk Territory and the Krasnoyarsk Science Foundation project No. 23-22-10016.

Conflict of interest

The authors declare that they have no conflict of interest.

References

- [1] D. Yang, F. Wang, Y. Ren, Y. Zuo, Y. Peng, S. Zhou, D. Xue. *Adv. Funct. Mater.* **23**, 23, 2918 (2013).
- [2] B. Cheng, H.W. Qin, J.F. Hu. *J. Phys. D* **50**, 445001 (2017).
- [3] S.S. Aplesnin, M.N. Sitnikov, A.M. Kharkov, H. Abdelbaki. *J. Mater. Sci.: Mater. Electron.* **34**, 284 (2023).
- [4] H. Boppart, P. Wachter. *Mater. Res. Soc. Symp. Proc.* **22**, 341 (1984).
- [5] P. Wachter. *Adv. Mater. Phys. Chem.* **8**, 120 (2018).
- [6] W. Reim, P. Wachter. *Phys. Rev. Lett.* **55**, 871 (1985).
- [7] E. Kaldis, B. Fritzler. *Prog. Solid. State. Chem.* **14**, 95 (1982).
- [8] S.S. Aplesnin, L.I. Ryabinkina, G.M. Abramova, O.B. Romanova, A.M. Vorotynov, D.A. Velikanov, N.I. Kiselev, A.D. Balaev. *Phys. Rev. B* **71**, 125204 (2005).
- [9] D. Schaller, P.G. LaBarre, T. Besara, A. Henderson, K. Wei, E. Bucher, T. Siegrist, A.P. Ramirez. *Phys. Rev. Mater.* **3**, 104602 (2019).
- [10] A. Sousanis, P.F. Smet, D. Poelman. *Materials* **10**, 953 (2017).
- [11] S.S. Aplesnin, O.B. Romanova, M.V. Gorev, D.A. Velikanov, A.G. Gamzatov, A.M. Aliev. *J. Phys. Condens. Matter* **25**, 025802 (2013).
- [12] S. Lee, J.-H. Kim, Y.-W. Kwon. *Condens. Matter. Supercond.* arXiv:2307.12008 (2023).
- [13] K.A. Kikoin, A.S. Mischenko. *ZhETF* **104**, 5, 3810 (1993). (in Russian).
- [14] P. Shvets, O. Dikaya, K. Maksimova, A. Goikhman. *J. Raman Spectrosc.* **50**, 8, 1226 (2019).
- [15] V.J. Singh, C.D. Bruneau, D. Chidambaram. *ECSarXiv* (2019).
- [16] T.T. Zhang, K.W. Li, J. Zeng, Y.L. Wang, X.M. Song, H. Wang. *J. Phys. Chem. Solids* **69**, 2845 (2008).
- [17] R.X. Silva, C.W.A. Paschoal, R.M. Almeida, M.C. Castro, A.P. Ayala, J.T. Auletta, M.W. Lufaso. *Vib. Spectrosc.* **64**, 172 (2013).
- [18] J. Hao, Y. Zhang, X. Wei. *Angew. Chem. Int. Ed.* **50**, 6876 (2011).
- [19] N.V. Minh, I.S. Yang. *Vib. Spectrosc.* **42**, 353 (2006).
- [20] M.N. Iliiev, A.P. Litvinchuk, V.G. Hadjiev, M.M. Gospodinov, V. Skumryev, E. Ressouche. *Phys. Rev. B* **81**, 024302 (2010).
- [21] T.A. Vanderah, I. Levin, M.W. Lufaso. *Eur. J. Inorg. Chem.* **14**, 2895 (2005).
- [22] V. Krayzman, I. Levin, J.C. Woicik. *Chem. Mater.* **19**, 932 (2007).
- [23] K.S. Aleksandrov, S.V. Misyul, M.S. Molochev, V.N. Voronov. *FTT* **51**, 12, 2359 (2009). (in Russian).
- [24] S.S. Aplesnin, L.I. Ryabinkina, G.M. Abramova, O.B. Romanova, N.I. Kiselyov, A.F. Bovina. *FTT* **46**, 11, 2000 (2004). (in Russian).
- [25] A.R. Long. *Adv. Phys.* **31**, 587 (1982).
- [26] A.D. Polushina, E.D. Obozova, V.G. Zalesky, T.A. Smirnova, S.G. Lushnikov. *FTT* **63**, 9, 1382 (2021). (in Russian).
- [27] M.M. Parish, P.B. Littlewood. *Phys. Rev. Lett.* **101**, 166602 (2008).
- [28] S.S. Aplesnin, O.B. Romanova, K.I. Yanushkevich. *Phys. Status Solidi B* **252**, 8, 1792 (2015).

Translated by Y.Alekseev